Numerical Modelling of Effect of Baffle Orientation Offset on Shell-And-Tube Heat Exchanger Performance

*Petinrin M. O. and Dare A. A.
Department of Mechanical Engineering, University of Ibadan, Ibadan, Nigeria
*Corresponding author: layopet01@yahoo.com, mo.petinrin@ui.edu.ng

Abstract
The performance of a shell-and-tube heat exchanger (STHE) is largely dependent on the type, orientation and offset arrangement of the baffles employed. In this paper, the thermal-hydraulic characteristics of STHEs with 90°, 120° and 180° offset arrangements of baffles were studied numerically. The study was performed on 19-tube and 31-tube heat exchangers, and also for three shell-side working fluids: air, water and engine oil. The numerical analyses were carried out using the *k-ε* model with imposed realizability constraint, and were solved with COMSOL Multiphysics. The STHE with 180° had higher pressure drop than other STHEs for all the ranges of mass flow rate. STHE with 120° showed better performance for shell-side heat transfer coefficient at the same pressure drop while STHE with 90° had much higher performance factor at the same mass flow rate. It is concluded that baffle offset arrangements significantly affected the shell and tube heat exchanger performance.

Index Terms: Shell-and-tube heat exchangers, heat transfer coefficient, pressure drop, baffle offset

1. INTRODUCTION

Shell-and-tube heat exchangers (STHEs) are the most frequently used type of heat exchangers for transferring heat from one fluid to another [1,2]. This is due to their adaptability for large operating pressures and temperatures ranges, and their simplicity of construction [3–5]. Applications of STHEs are not limited to oil refining, food industry, power plants, [6,7] waste heat recovery, petrochemical plants, transformer oil cooling, ethanol mash-stillage and air-conditioning [7,8]. Heat exchanger design and its effectiveness have significant impact on the overall energy requirement of a system [10].

Baffles are placed in STHEs to improve the performance of the heat exchangers by enhancing the heat transfer between the interacting fluids through the tortuous motion of fluid on the shell-side. They also provide supports for the internal structure of the heat exchangers such as the tubes against flow-induced vibrations and sagging [11]. Different types of baffles are being employed in heat exchangers, such as the segmental (single, double and triple), rod, helical and grid baffles. Although, the other types of baffles, most especially the helical baffles have reportedly demonstrated good performance with much lower pressure drop than the segmental baffles, but are associated with lower heat transfer performance and higher manufacturing costs [12–14]. The single-segmental baffles are the predominantly used due to their higher heat transfer enhancement capability. However, the inclination and orientation of these baffles have pronounced effect on the performance of STHEs [15-16].

Single-segmental baffles can be arranged with an inclination angle to the tube bundles to improve on fouling and minimise the pressure drop. From the experimental work reported by Kumar et al. [17] on 0°, 15°, 30° and 45° inclination angles, the heat transfer rate increased up to 30° and dropped at 45° while the pressure drop slid down from 0° to 45° inclination angle. In the numerical analysis carried out by Raj and Ganne [12] for inclination angles of 0°, 10°, and 20°, it was discovered that the 20° inclination angle offered better performance than others.

Segmental baffles can be categorized as perpendicular, parallel and inclined depending on the orientation of the baffle cut to shell inlet or nozzle axis (Figure 1) [18]. Some authors also grouped them accordingly as horizontal, vertical and rotated [15,16,19]. The horizontal (perpendicular-cut) baffles are always preferred for single-phase service on the shell-side to minimise deposit accumulation on the lower part of the shell and cause improvement of the flow distribution in the inlet and outlet zones [18,19]. However, the vertical (parallel-cut) baffles are more appropriate for condensing fluids [15,18].

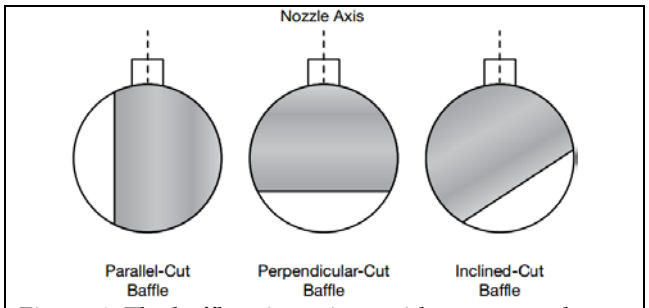

Figure 1. The baffle orientations with respect to the nozzle axis

Mohammadi et al. [20] conducted a numerical study on effects of baffle orientation on heat flow and heat transfer characteristics of STHEs. They found that for STHEs without leakage flow that the horizontal baffle is more desirable as its shell-side heat transfer coefficient to pressure drop ratio, that is the performance ratio, was

more than that of the vertical baffle. However, when the same series of studies were performed on STHEs with leakage flow, the vertical orientation was more advantageous except for performance at the inlet and outlet zones. They reported that there was up to 250% greater in pressure drop of the horizontal than the vertical baffle orientation while the heat transfer coefficient was just about 25% higher.

Mohammadi et al. [21] performed another numerically investigated the effect of orientation of baffles in a heat exchanger with leakage flow using three shell-side fluids (air, water and engine oil) each at a time. They observed that the vertical baffle seemed to have better performance in terms of the heat transfer to pressure ratio than the horizontal baffles, and this was more noticeable with air as a shell-side fluid.

It has been established from previous studies, as it can be seeing from the reviewed literatures, that the baffle orientations have significant effect on STHEs performance; however, as it had been noticed before carrying out this study, that studies of combined use of any of the baffle orientations in a single shell-and-tube heat exchanger have not been reported in the literature. Therefore, in this present study, the combined arrangements of the baffle orientations (parallel, perpendicular and inclined) on the performance of STHEs are numerically investigated and compared with the horizontal baffle shell-and-tube heat exchangers. Also, the effect of two different numbers of tubes as they affect this comparison is considered.

2. MATHEMATICAL MODELLING

In this section, the implementation steps for the simulations are discussed.

2.1. Basic Data for the Simulation

The geometrical data of the computational model of the STHE under study are presented in Table 1. The heat exchanger baffles were arranged with adjacent baffles offsetting at 90° (STHE/90d), 120° (STHE/120d) and 180° (STHE/ST, the standard) (Figure 2). The thermophysical properties of the working fluids were varied with the temperature of the fluids. Water was selected as the tube-side working fluid while air, water and engine oil were used on the shell-side at separate runs. However, heat exchangers with 31 tubes had only the engine oil on the shell-side. The mass flow rate of water on the tube-side was fixed as 0.3 kg/s while on the shell-side; the mass flow rates of water and engine oil were ranged 0.10-3.10 kg/s, and the air was ranged 0.0025-0.0325 kg/s. These were chosen based on the practical range of velocities found in the literature [15,22].

Table 1. The geometrical data of the shell and tube heat exchanger

Parameter	Value
Shell diameter	108.06 mm
Shell duct diameter	30.00 mm
Baffle cut	25%
Baffle spacing	43.26 mm
Baffle number	6
Offset between adjacent baffles	90°, 120° and 180° (standard, horizontal baffle)
Tube number	19 and 31
Tube diameter	15.88 mm and 12.70 mm
Tube pitch ratio	1.25
Tube layout	Triangular (30°)

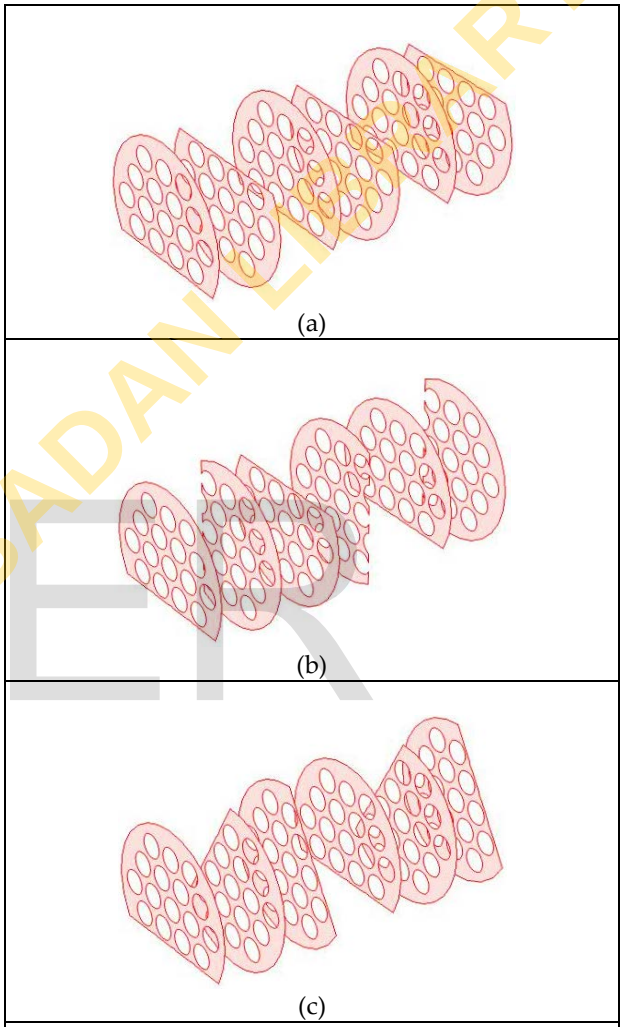

Figure 2. The baffle arrangements for (a) STHE/ST, (b) STHE/90d and (c) STHE/120d

2.2. Governing Equation

The *k-ε* model was adopted for the computational analysis because of its robustness and fair accuracy in approximating turbulent flow problems [23]. Thus, the governing equations for the fluid flow and heat transfer within the STHEs as given by Wilcox [24] and Tannehill et al. [25] are:

Continuity Equation

$$\frac{\partial\left(\bar{\rho}\tilde{u}_j\right)}{\partial x_j}=0 \qquad (1)$$

Momentum equation:

$$\frac{\partial\left(\bar{\rho}\tilde{u}_j\tilde{u}_i\right)}{\partial x_j}=-\frac{\partial\bar{p}}{\partial x_i}+\frac{\partial}{\partial x_j}\left[\left(\mu+\mu_T\right)\left(\left(\frac{\partial\tilde{u}_i}{\partial x_j}+\frac{\partial\tilde{u}_j}{\partial x_i}\right)-\frac{2}{3}\delta_{ij}\frac{\partial\tilde{u}_k}{\partial x_k}\right)-\frac{2}{3}\bar{\rho}k\delta_{ij}\right] \quad (2)$$

Energy equation:

$$\frac{\partial}{\partial x_j}\left(\bar{\rho}c_p\tilde{T}\tilde{u}_j\right)=\frac{\partial}{\partial x_j}\left(\left(\eta+\eta_T\right)\frac{\partial\tilde{T}}{\partial x_j}\right) \quad (3)$$

Turbulent kinetic energy:

$$\frac{\partial\left(\bar{\rho}k\tilde{u}_j\right)}{\partial x_j}=\frac{\partial}{\partial x_j}\left[\left(\mu+\frac{\mu_T}{\sigma_k}\right)\frac{\partial k}{\partial x_j}\right]+P_k-\bar{\rho}\varepsilon \quad (4)$$

Turbulent dissipation energy:

$$\frac{\partial\left(\bar{\rho}\varepsilon\tilde{u}_j\right)}{\partial x_j}=\frac{\partial}{\partial x_j}\left[\left(\mu+\frac{\mu_T}{\sigma_\varepsilon}\right)\frac{\partial\varepsilon}{\partial x_j}\right]+C_{\varepsilon1}\frac{\varepsilon}{k}P_k-C_{\varepsilon2}\rho\frac{\varepsilon^2}{k} \quad (5)$$

while the production term, P_k in equations 4 and 5 is

$$P_k=\frac{\partial\tilde{u}_i}{\partial x_j}\left[\mu_T\left(\left(\frac{\partial\tilde{u}_i}{\partial x_j}+\frac{\partial\tilde{u}_j}{\partial x_i}\right)-\frac{2}{3}\delta_{ij}\frac{\partial\tilde{u}_k}{\partial x_k}\right)-\frac{2}{3}\bar{\rho}k\delta_{ij}\right] \quad (6)$$

The closure constants are:
$C_{\varepsilon1}$ = 1.44, $C_{\varepsilon2}$ = 1.92, C_μ = 0.09, σ_k = 1.0 and σ_ε = 1.3.

2.3. Initial and Boundary Conditions

The initial velocities of the working fluids were set as zero while the initial pressures were equalised to atmospheric pressure. Also, the fluids initial temperature was 303.15 K. Velocity-inlet conditions were set at the inlets to the tube- and shell-sides of the heat exchangers. The temperatures at the tube and shell inlets were 303.15 K and 373.15 K respectively. Outflow boundary conditions were applied at the outlets with pressure at atmospheric pressure. Wall functions were applied at the tube and shell walls, and baffle surfaces to avert resolving the strong sharp velocity and temperature gradients close to the walls. Also by assuming the shell wall was insulated, the loss of heat to the surroundings was considered to be negligible.

2.4. Mesh Generation and Numerical Method

The computational domains were discretised into unstructured tetrahedral elements of averagely 70,175 and 124,566 for the 19- and 31-tubes heat exchangers respectively (Figure 3). The equations governing the heat exchanger models were solved with COMSOL Multiphysics based on finite element method. The streamline diffusion (streamline-upwind Petrov-Galerkin., SUPG and Galerkin Least-Square, GLS), and crosswind diffusion were employed to enhance the accuracy and stability of the analyses [30,31]. Three segregated solvers were used to obtain solutions to the primitive variables. There were two iterative solvers, the GMRES (preconditioner: Incomplete LU) for velocity and pressure, and temperature. A direct solver, MUMPS was selected for the turbulent kinetic energy and rate of dissipation for its robustness and efficiency [28].

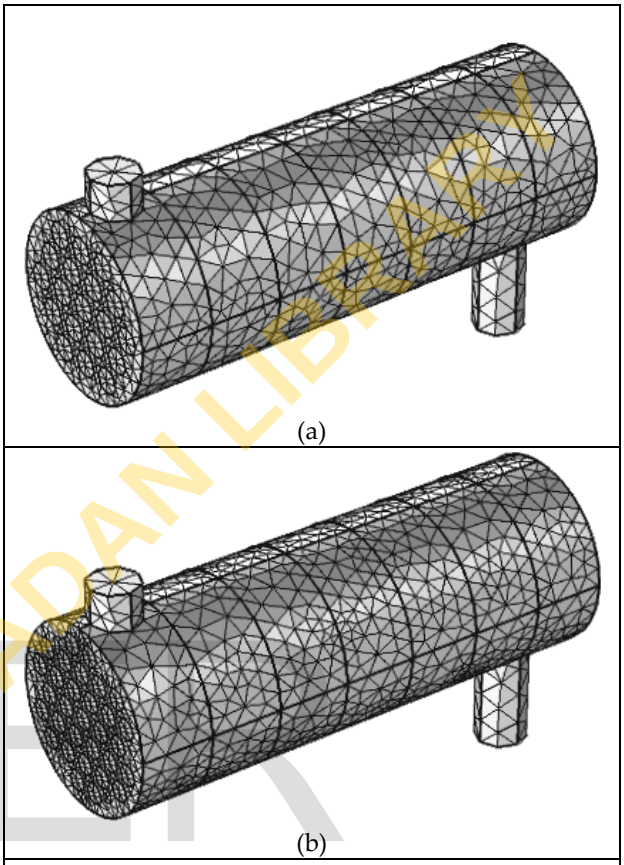

Figure 3. The finite element mesh grid for (a) 19-tube STHE and (b) 31-tube STHE

3. Performance Indices and Naming Conventions of Heat Exchangers

Two methods were used in assessing the performance of each heat exchanger in this study as compared against heat exchanger with horizontal baffle (180°) arrangement. The first method evaluated the equivalent shell-side heat transfer coefficient of each heat exchanger at the same pressure drop with the horizontal-baffle (180°) heat exchanger [12,13].

In the second method, performance factor was determined by dividing the shell gain factor of any STHE against that of STHE with standard baffle offset for the same mass flow rate or Reynolds number. The shell gain factor, Γ for each heat exchanger as obtained from Mohammadi et al. [21] was evaluated as

$$\Gamma=\frac{h}{\Delta p} \quad (10)$$

where h is the shell-side heat transfer coefficient and Δp is the pressure drop of the fluid across the shell-side of the heat exchanger.

Hence, the performance factor of a heat exchanger with a more desirable baffle offset should be greater than

one if operating at the same mass flow rate or Reynolds number as the heat exchanger with horizontal baffle.

The naming conventions adopted to represent the graphical plots for all the offset arrangements of baffles, tube numbers and working fluids for easy interpretation are as shown in Figure 3.

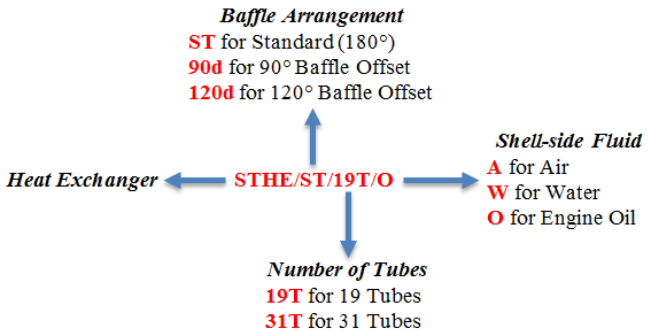

Figure 3. The naming convention for interpreting graphical plots

4. RESULTS AND DISCUSSION

The flow streams of the shell-side fluid (engine oil) at a mass flow rate of 3.10 kg/s for the different baffle offsets are as shown in Figure 4. It can be observed that the fluid flow paths are influenced by the offsets of the baffles and each pair of baffle offset for 19- and 31-tubes heat exchangers have the same flow behaviour. The flow through the STHE/ST (standard) exhibits a zigzag cross-flow movement over the tube bundles while the other offsets have crisscross flow distribution. For all arrangements, the fluid velocities reduce from the shell-inlet into the shell and then rise again at the shell-outlet. This is because the law of conservation of mass must be obeyed; the flow area between the shell and all the tubes is much greater than those at shell inlet and outlet.

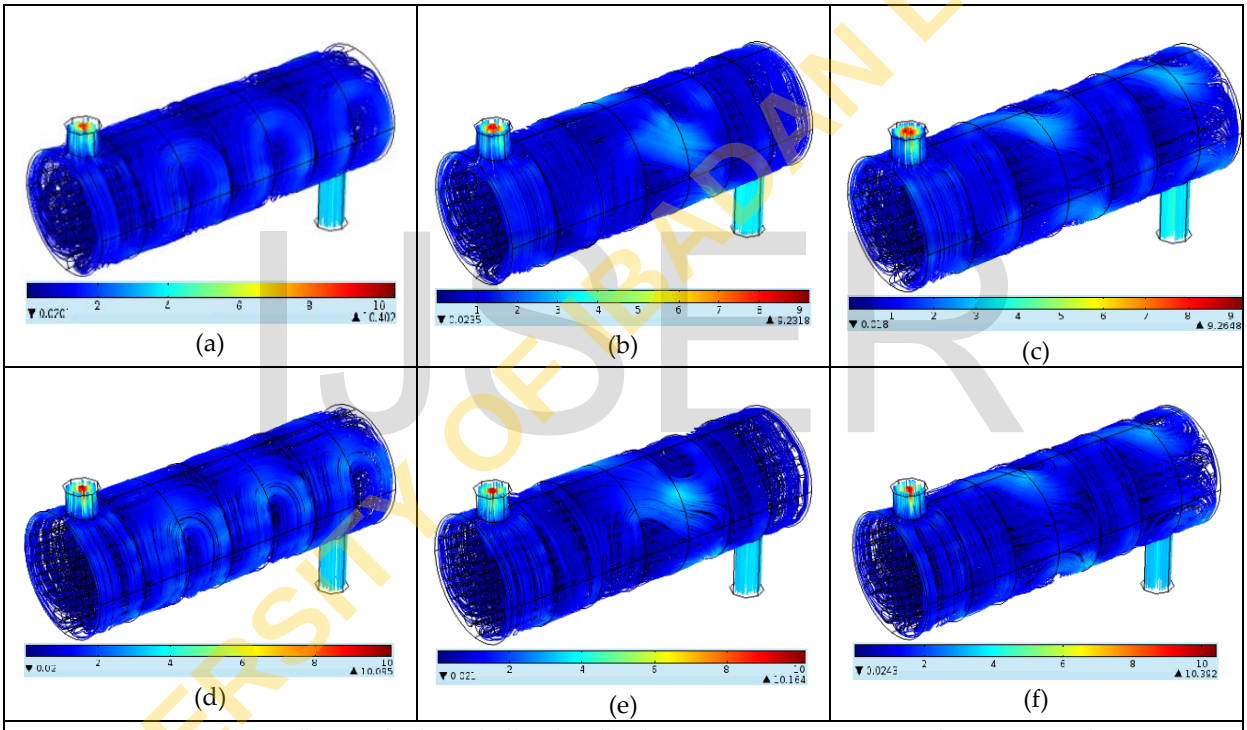

Figure 4. Streamline flow of the shell-side fluid (a) STHE/ST/19T/O, (b) STHE/90d/19T/O, (c) STHE/120d/19T/O, (d) STHE/ST/31T/O, (e) STHE/90d/31T/O and (f) STHE/120d/31T/O

The plots of the shell-side heat transfer coefficient versus the Reynolds number are as shown in Figure 5. It can be seen that for each STHE baffle offset and working fluid, the heat transfer coefficient increases with the Reynolds number, which also corresponds to the increase in the mass flow rate of each of the fluid. However, for water and engine oil, the increment rates of their heat transfer coefficients tend to reduce at higher Reynolds numbers while linear increment was observed for air. This is partly due to the physical nature of each fluid. The shell-side heat transfer coefficients of STHE/90d/19T/A and STHE/120d/19T/A for the ranges of Reynolds numbers considered are -4.26% and 2.32%, respectively on average greater than STHE/ST/19T/A. STHE/90d/19T/W and STHE/120d/19T/W are greater with -4.06% and 3.93% than STHE/ST/19T/W, respectively. The corresponding values of STHE/90d/19T/O and STHE/120d/19T/O are -7.39% and 0.03% greater than STHE/ST/19T/O, respectively. Thus, all the STHE/120d have better shell-side heat transfer coefficients than others. This same trend can be observed as indicated in Figure 6 for STHEs with 19 and 31 tubes. It can equally be observed that the heat transfer coefficients for all the 31-tube STHEs are greater than those of 19-tube STHEs, this is partly due to the fact that the 31-tube STHEs have more surface area for heat exchange between the working fluids on both sides of the tubes.

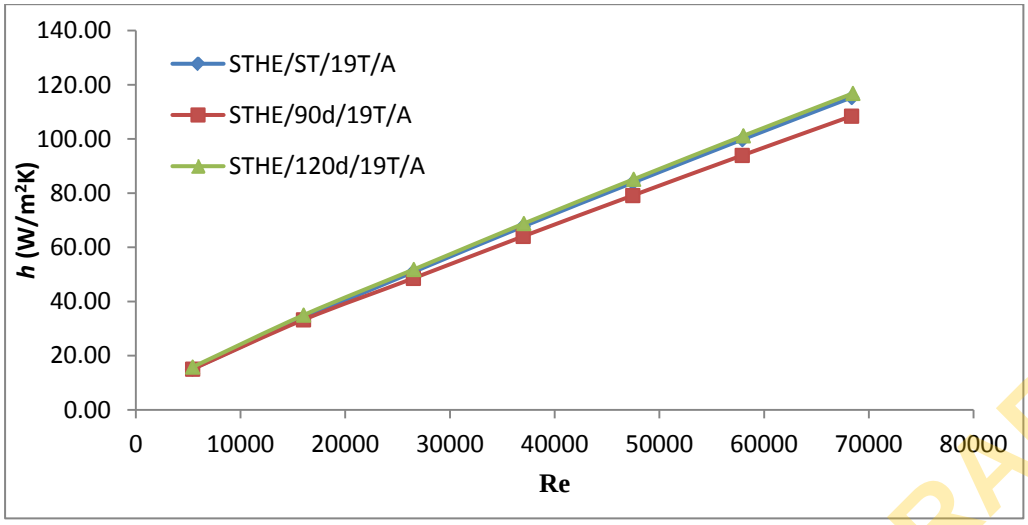

(a) Shell-side working fluid: air

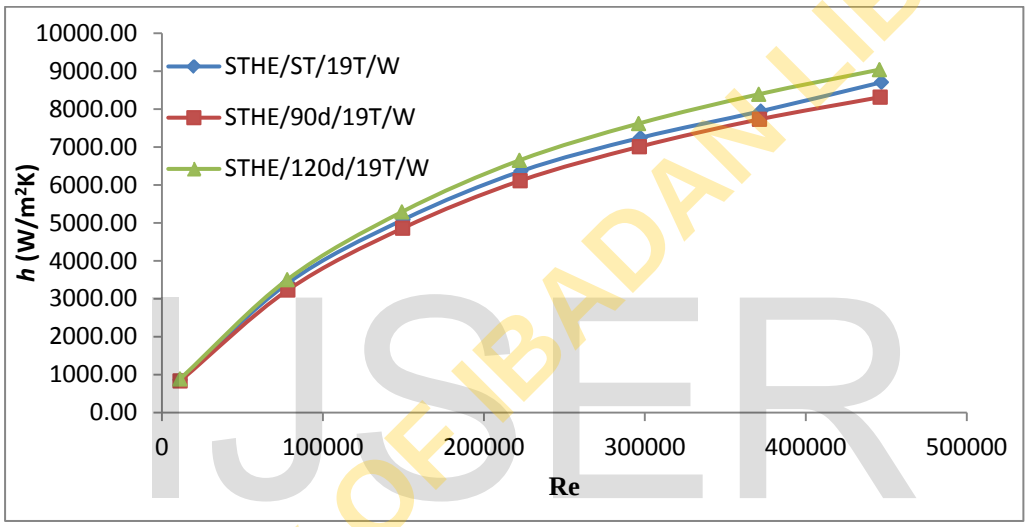

(b) Shell-side working fluid: water

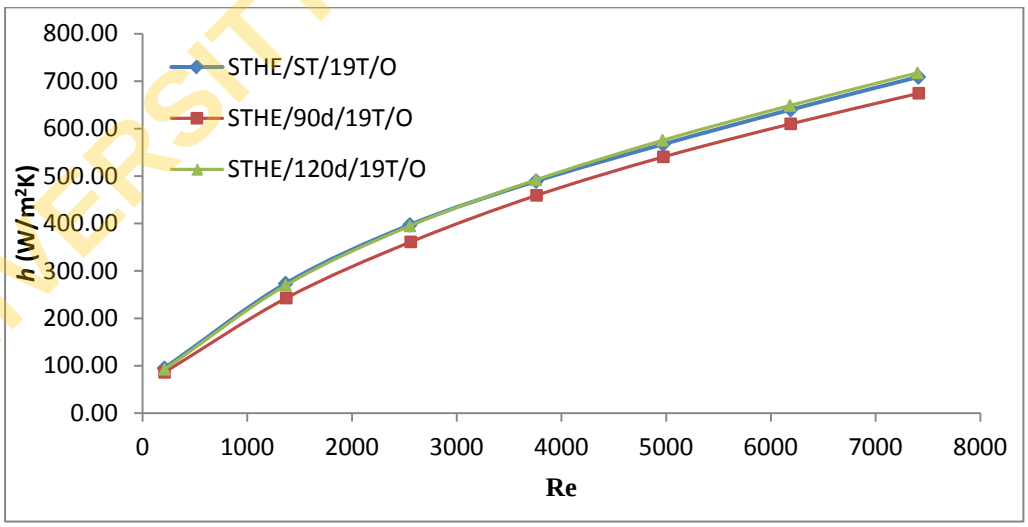

(c) Shell-side working fluid: engine oil

Figure 5. Shell-side heat transfer coefficient versus Reynolds number (19-tube heat exchangers)

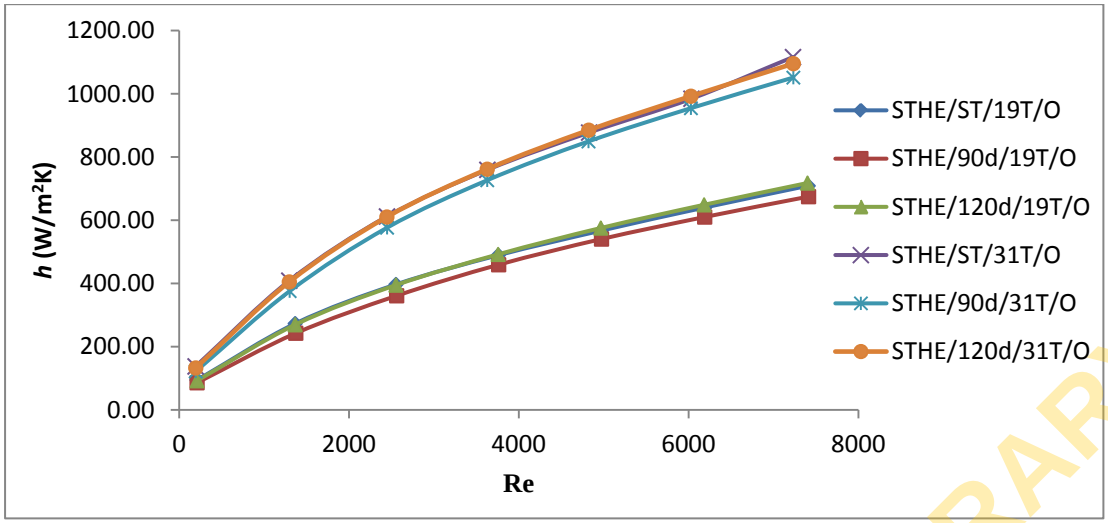

Figure 6. Shell-side heat transfer coefficient versus Reynolds number (19- and 31-tubes heat exchangers)

The variations of the shell-side Nusselt number for each fluid against the Reynolds number for all heat exchangers are as indicated in Figure 7. The trends in these figures are similar to those for heat transfer coefficients showed in Figure 5 for each working fluid.

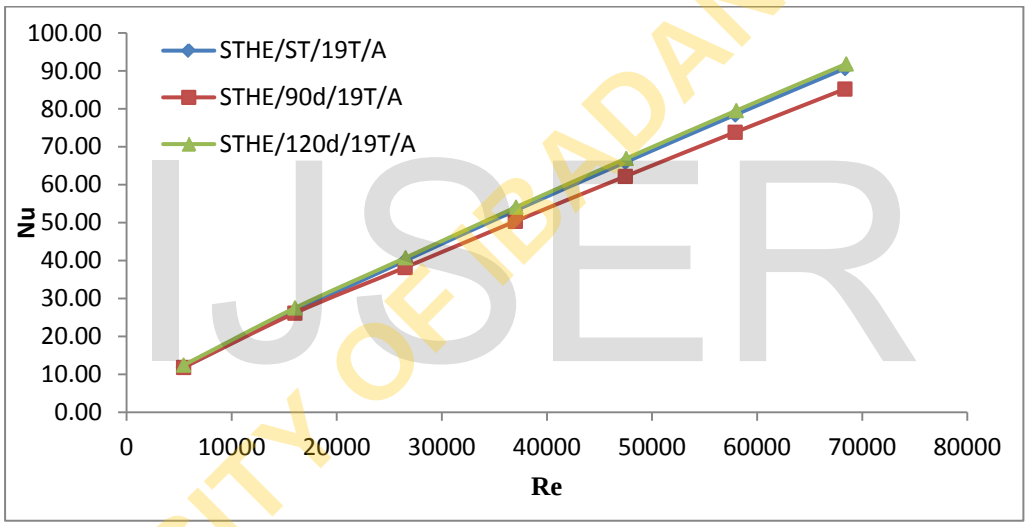

(a) Shell-side working fluid: air

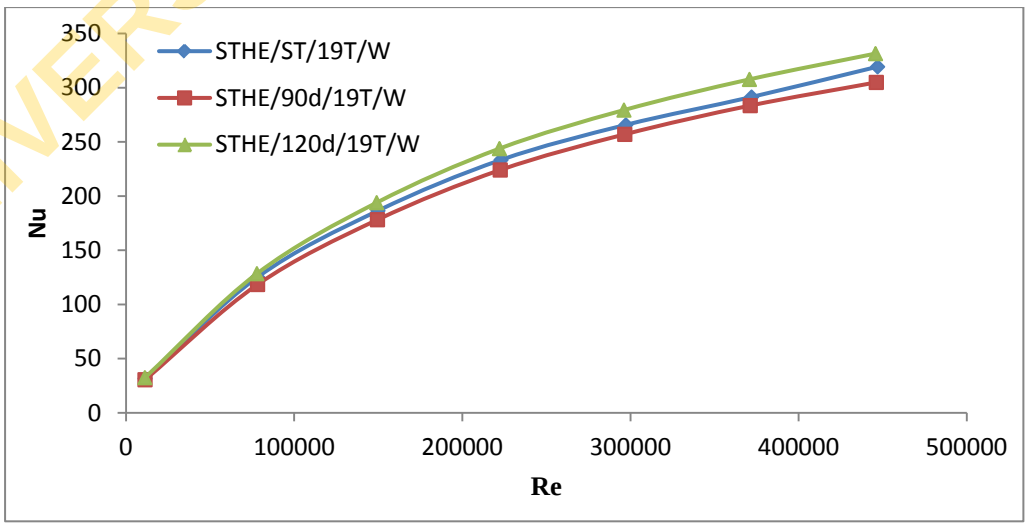

(b) Shell-side working fluid: water

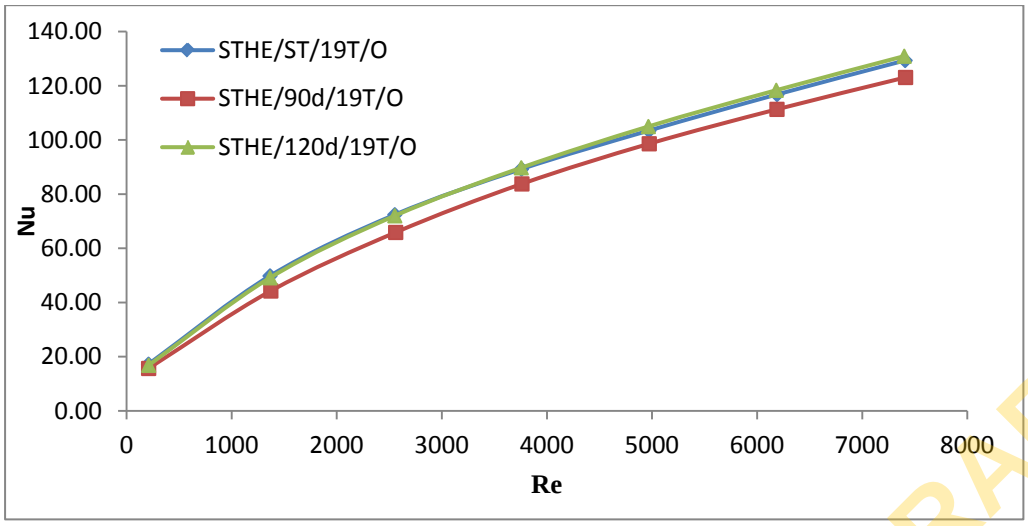

(c) Shell-side working fluid: engine oil

Figure 7. Nusselt number versus Reynolds number (19-tube heat exchangers)

Figure 8 shows the shell-side pressure drop versus the Reynolds number for the heat exchangers. The pressure drop increases rapidly with the increase in the Reynolds number. These trends were also observed in the studies conducted by Wang et al. [13] and Yang et al. [4]. Within the range of Reynolds number studied, the shell-side pressure drop of STHE/90d/19T/A and STHE/120d/19T/A are averagely lower than that of STHE/ST/19T/A by 19.76% and 5.30%, respectively. The STHE/90d/19T/W and STHE/120d/19T/W are lower than STHE/ST/19T/W by 18.18% and 3.93%, respectively. The pressure drop of STHE/90d/19T/O and STHE/120d/19T/O are 23.99% and 7.77% lower than STHE/ST/19T/O, respectively. This implies that all the STHE/ST demonstrate higher pressure on the shell-side, which can be attributed to the zigzag cross-flow motion of the fluid over tube bundles. Similar trends as observed in Figure 8 are also depicted in Figure 9. In Fig 9, the pressure drops across all the 31-tube heat exchangers are more pronounced than those of 19-tube heat exchangers with a lower surface area of shell-side working fluid interaction with the tubes.

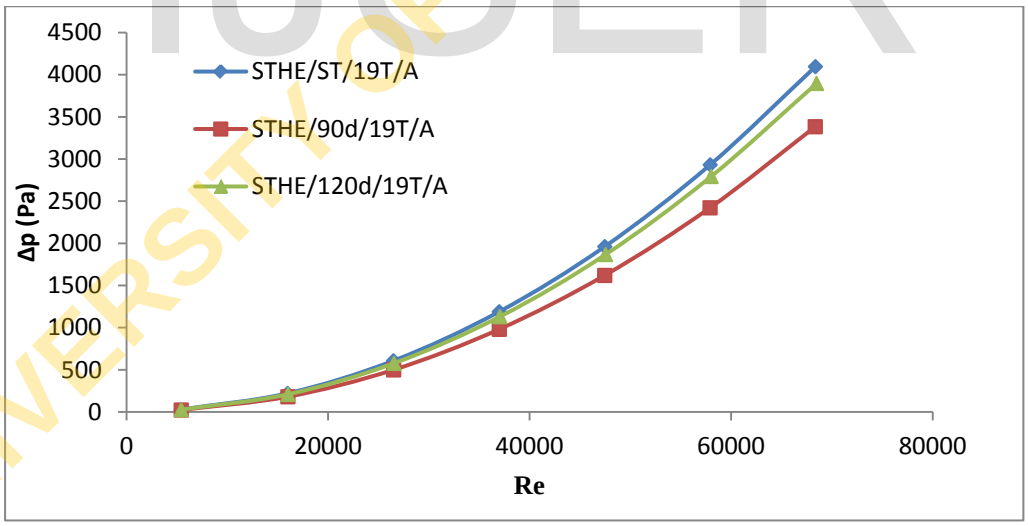

(a) Shell-side working fluid: air

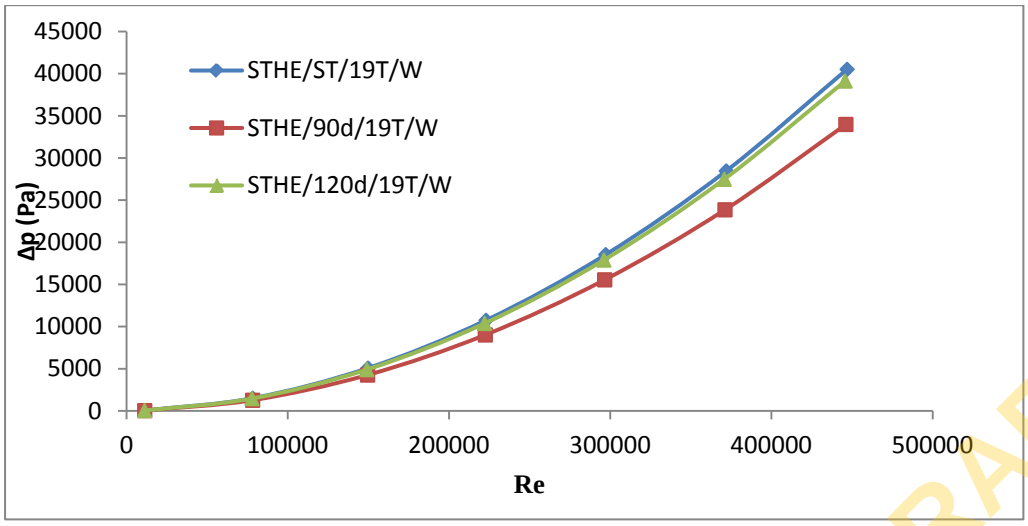

(b) Shell-side working fluid: water

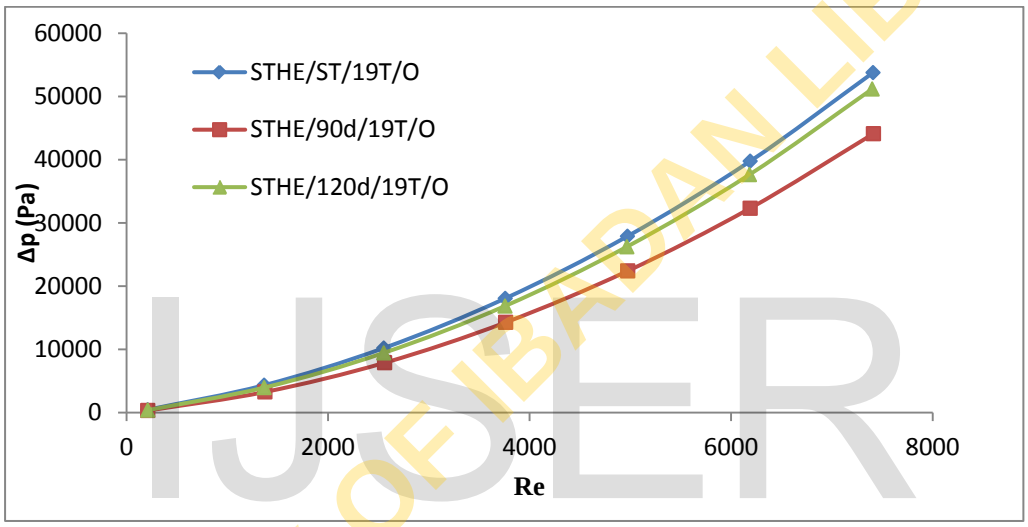

(c) Shell-side working fluid: engine oil

Figure 8. Shell-side pressure drop versus Reynolds number (19-tube heat exchangers)

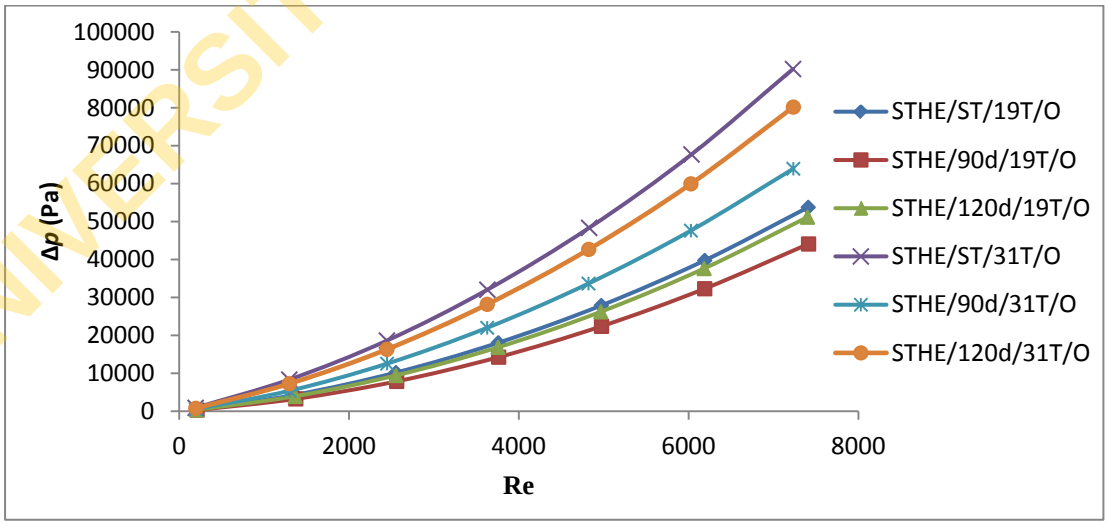

Figure 9. Shell-side pressure drop versus Reynolds number (19- and 31-tubes heat exchangers)

The variations of the shell-side heat transfer coefficient of the heat exchangers with the overall pressure drops are presented in Figure 10. There are indications from the plots that the pressure drop increases more rapidly than the increase in the corresponding heat transfer coefficient with increasing mass flow rate. Evaluating the shell-side heat transfer coefficient of STHEs at the same pressure drop, the STHE/120d shows better performance. The heat transfer coefficient of STHE/90d/19T/A and STHE/120d/19T/A are

averagely greater than that of STHE/ST/19T/A by 2.79% and 4.13%, respectively. The STHE/90d/19T/W and STHE/120d/19T/W are higher with 0.36% and 4.67% than STHE/ST/19T/W, respectively. While in the same order, STHE/90d/19T/O and STHE/120d/19T/O are 0.53% and 1.05% greater than STHE/ST/19T/O. Similar trends for all the baffle offsets are observed in Figure 11 for 31-tube heat exchangers. It can also be seen from this plot that the 31-tube STHEs exhibit better performance with higher heat transfer coefficient for the same pressure drop than the 19-tube STHEs. This implies a gain in heat transfer with increased surface area for the energy expended.

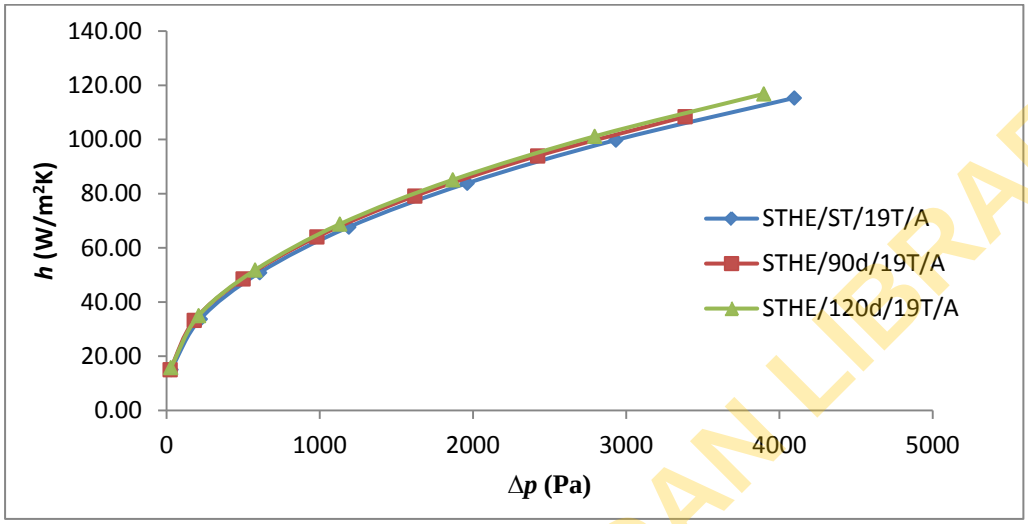

(a) Shell-side working fluid: air

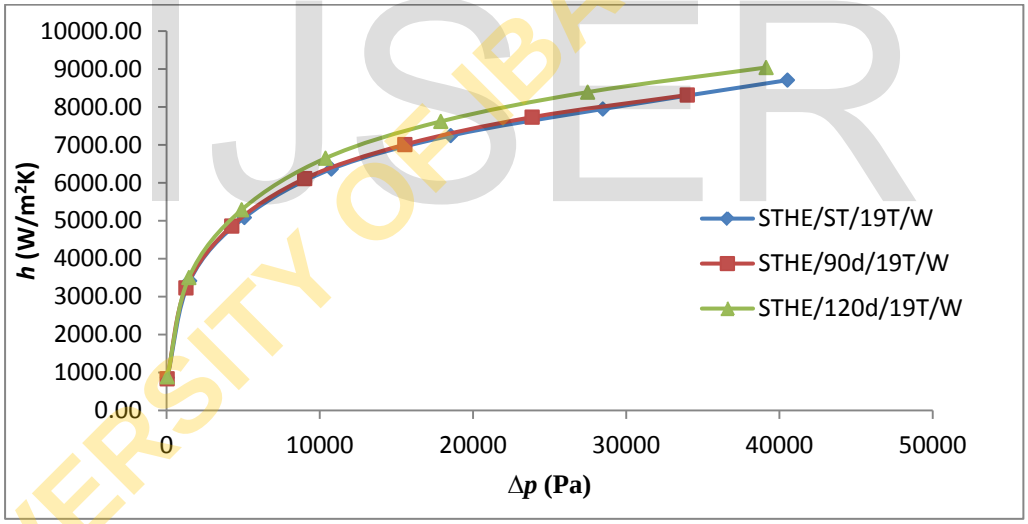

(b) Shell-side working fluid: water

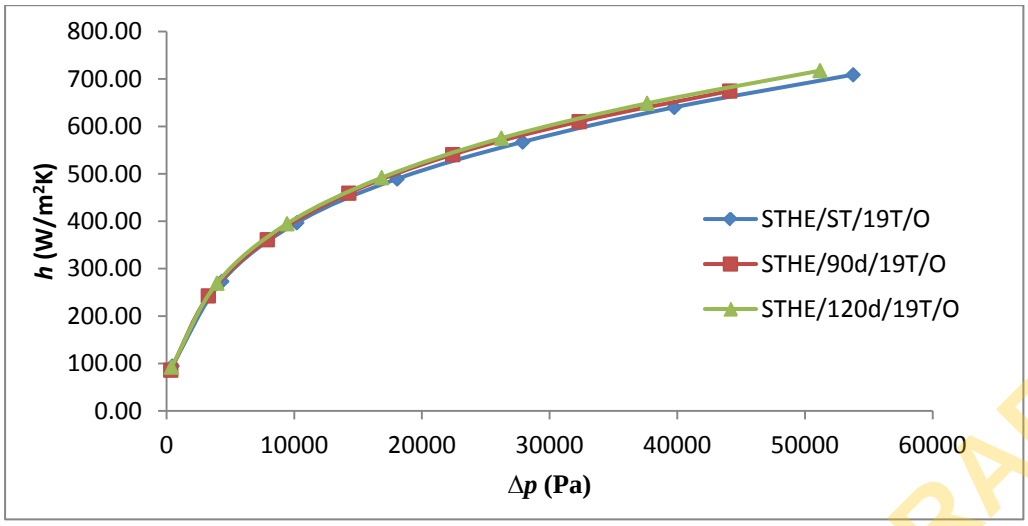

(c) Shell-side working fluid: engine oil

Figure 10. Shell-side heat transfer coefficient versus pressure drop (19-tubes heat exchangers)

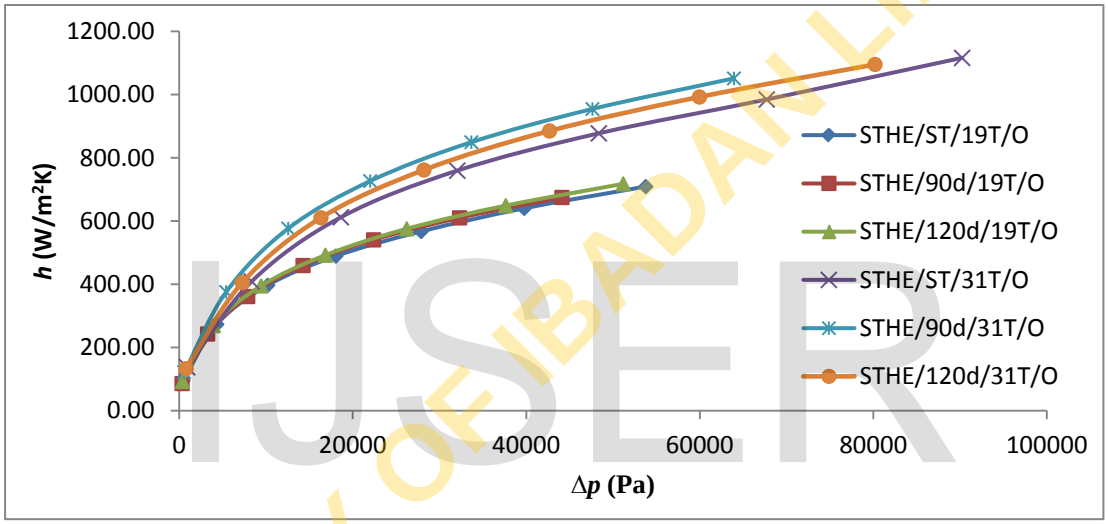

Figure 11. Shell-side heat transfer coefficient versus pressure drop (19- and 31-tubes heat exchangers)

The plots of the performance factors of the STHEs at varying Reynolds number are as shown in Figure 12. It can be observed that for all the working fluid in Figure 12, the STHE/90d has the best performance factor at the same Reynolds number. Averagely, the performance factor of STHE/90d/19T/A and STHE/120d/19T/A are greater than that of STHE/ST/19T/A by 15.53% and 7.62%, respectively. The STHE/90d/19T/W and STHE/120d/19T/W are higher with 14.15% and 7.87% than STHE/ST/19T/W, respectively. The performance factor of STHE/90d/19T/O and STHE/120d/19T/O are 16.68% and 7.81% higher than STHE/ST/19T/O in that order. Figure 13 shows the same trend for 31-tube heat exchangers. For same baffle offsets, the 31-tube heat exchangers have higher performance factors than the 19-tube heat exchangers.

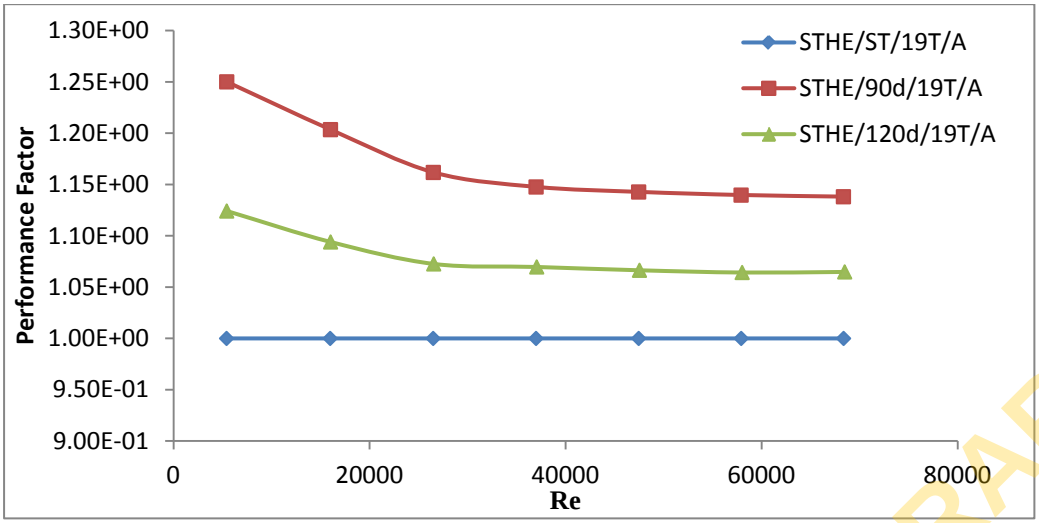

(a) Shell-side working fluid: air

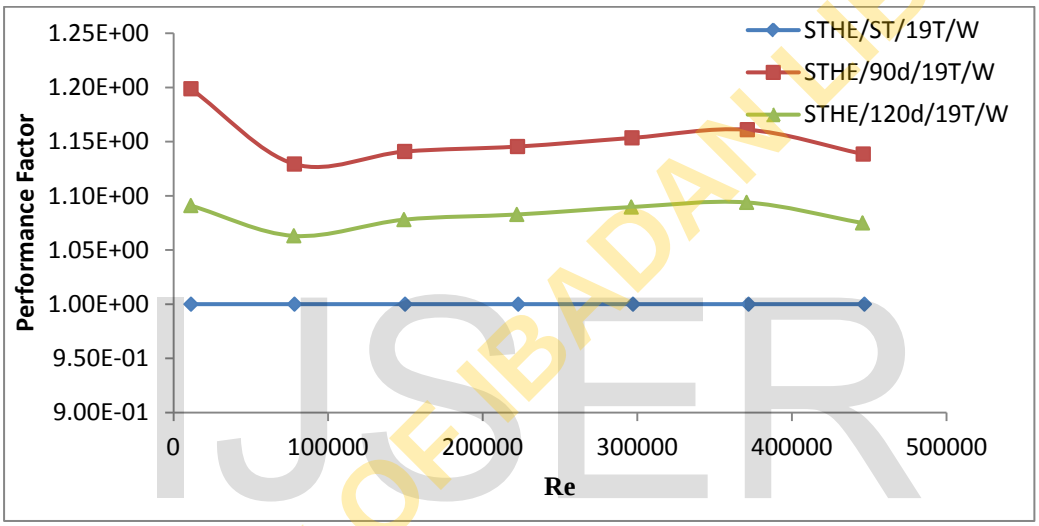

(b) Shell-side working fluid: water

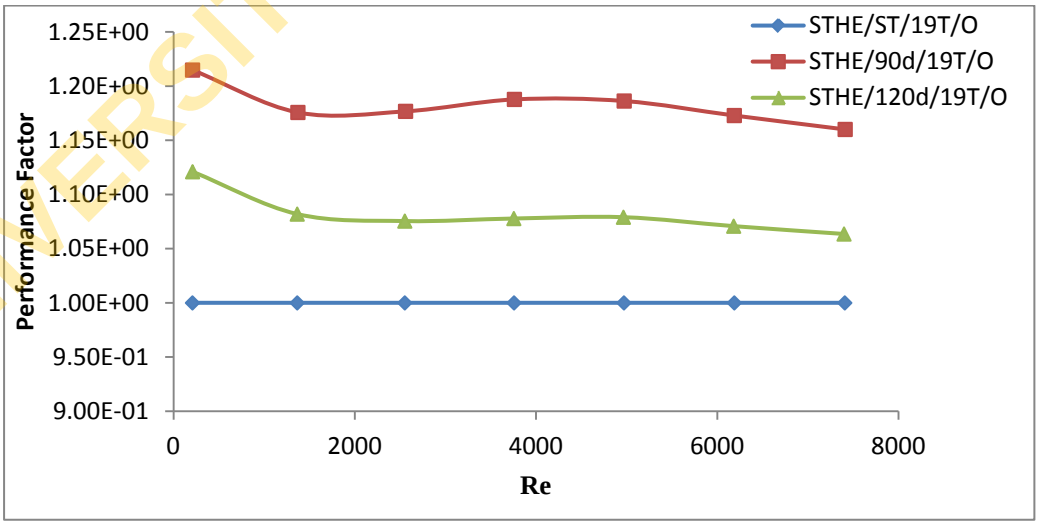

(c) Shell-side working fluid: engine oil

Figure 12. Performance factor versus Reynolds number (19-tubes heat exchangers)

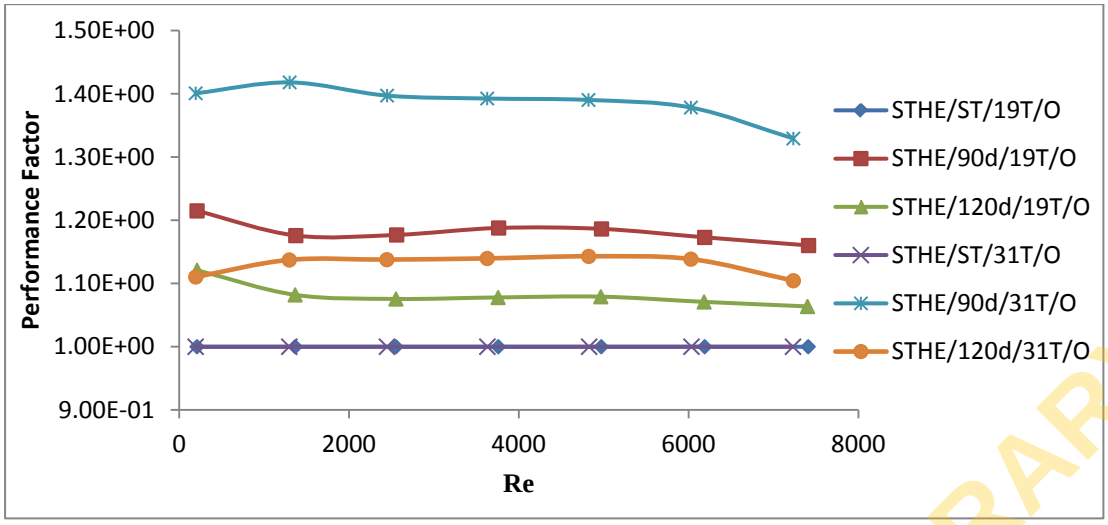

Figure 13. Performance factor versus Reynolds number (19- and 31-tubes heat exchangers)

5. CONCLUSION

In this study, the thermal-hydraulic performance of three baffle arrangements in shell-and-tube heat exchangers has been carried out using the numerical approach. The three-dimensional models of the heat exchangers were solved using the COMSOL Multiphysics CFD code. For all the shell-side working fluids and the ranges of mass flow rates considered, the STHEs with 180° offsets (horizontal) are characterised with higher pressure drop than STHEs with other baffle offsets, this is as a result of zigzag movement of shell-side fluid caused by the arrangement of the 180° offsets. Assessing the performance of baffle arrangements based on the heat transfer coefficient at the same pressure drop, the 120° offset baffles are more desirable in heat exchangers than others while the 180° offset baffles have poorer performance. However, the 90° offset baffles are more suitable than other offset arrangements, using the performance factor at the same Reynolds number or mass flow rate while the 180° offset baffles still exhibit much lower performance. For each corresponding baffle offset and the two performance criteria used, the 31-tube heat exchangers are better than the 19-tube heat exchangers because of the increased surface area of tubes. It is thus concluded that baffle offsets and tube numbers significantly affected the performance of shell and tube heat exchangers.

REFERENCES

[1] H. Li and V. Kottke, "Analysis of local shellside heat and mass transfer in the shell-and-tube heat exchanger with disc-and-doughnut baffles," *Int. J. Heat Mass Transf.*, vol. 42, pp. 3509–3521, 1999.

[2] M. A. Habib, M. Ben-Mansour, H. M. Badr, S. A. M. Said, and S. S. Al-Anizi, "Erosion in the tube entrance region of a shell and tube heat exchanger," *Int. J. Numer. Methods Heat Fluid Flow*, vol. 15, no. 2, pp. 143–160, 2005.

[3] B. K. Soltan and E. Damangir, "Minimizing capital and operating costs of shell and tube condensers using optimum baffle spacing," *Appl. Therm. Eng.*, vol. 24, pp. 2801–2810, 2004.

[4] J. Yang, M. Zeng, and Q. Wang, "Numerical investigation on combined single shell-pass shell-and-tube heat exchanger with two-layer continuous helical baffles," *Heat Mass Transf.*, vol. 84, pp. 103–113, 2015.

[5] J. Zhang, S. Guo, Z. Li, J. Wang, Y. He, and W. Tao, "Experimental performance comparison of shell-and-tube oil coolers with overlapped helical baffles and segmental baffles," *Appl. Therm. Eng.*, vol. 58, no. 1–2, pp. 336–343, 2013.

[6] B. Peng *et al.*, "An Experimental Study of Shell-and-Tube Heat Exchangers With Continuous Helical Baffles," *J. Heat Transfer*, vol. 129, pp. 1425–1431, 2007.

[7] W. Yongqing, G. Xin, W. Ke, and D. Qiwu, "Procedia Engineering Numerical investigation of shell-side characteristics of H-shape baffle heat exchanger," *Procedia Eng.*, vol. 18, pp. 53–58, 2011.

[8] M. M. Aslam Bhutta, N. Hayat, M. H. Bashir, A. R. Khan, K. N. Ahmad, and S. Khan, "CFD applications in various heat exchangers design: A review," *Appl. Therm. Eng.*, vol. 32, no. 1, pp. 1–12, 2012.

[9] B. Parikshit, K. R. Spandana, V. Krishna, T. R. Seetharam, and K. N. Seetharamu, "A simple method to calculate shell side fluid pressure drop in a shell and tube heat exchanger," *Int. J. Heat Mass Transf.*, vol. 84, pp. 700–712, 2015.

[10] Nasiruddin and M. H. K. Siddiqui, "Heat transfer augmentation in a heat exchanger tube using a baffle," *Int. J. Heat Fluid Flow*, vol. 28, no. 2, pp. 318–328, 2007.

[11] A. A. Shrikant, R. Sivakumar, N. Anantharaman, and M. Vivekenandan, "CFD simulation study of shell and tube heat exchangers with different baffle segment configurations," *Appl. Therm. Eng.*, vol. 108, pp. 999–1007, 2016.

[12] R. T. K. Raj and S. Ganne, "Shell side numerical analysis of a shell and tube heat exchanger considering the effects of baffle inclination angle on fluid flow," *Therm. Sci.*, vol. 16, no. 4, pp. 1165–1174, 2012.

[13] Q. Wang, Q. Chen, G. Chen, and M. Zeng, "Numerical investigation on combined multiple shell-pass shell-and-tube heat exchanger with continuous helical baffles," *Int. J. Heat Mass Transf.*, vol. 52, no. 5–6, pp. 1214–1222, 2009.

[14] Q. Wang *et al.*, "Shell-side heat transfer enhancement for shell-and-tube heat exchangers by helical baffles," *Chem. Eng. Trans.*, vol. 21, pp. 217–222, 2010.

[15] T. Kuppan, *Heat Exchanger Design Handbook, Second Edition*, 2nd ed. Boca Raton: Taylor and Francis, 2013.

[16] R. K. Shah and D. P. Sekulic, *Fundamentals of heat exchanger design*. Hoboken: John Wiley & Sons, 2003.

[17] P. Kumar, V. Kumar, and S. Nain, "Experimental Study on Heat Enhancement of Helixchanger with Grooved Tubes," *Int. J. Latest Trends Eng. Technol.*, vol. 3, no. 4, pp. 213–219, 2014.

[18] S. Bouhairie, "Selecting Baffles for Shell-and-Tube Heat Exchangers," *Heat Transf.*, pp. 27–33, 2012.

[19] R. Mukherjee, *Effectively design shell-and-tube heat exchangers*. 1998.

[20] K. Mohammadi, W. Heidemann, and H. Müller-Steinhagen, "Effect of Baffle Orientation on Heat Transfer and Pressure Drop of Shell and Tube Heat Exchangers with and without Leakage Flows," in *Proceedings of CHT-08 ICHMT International Symposium on Advances in Computational Heat Transfer*, 2008.

[21] K. Mohammadi, W. Heidemann, and H. Müller-Steinhagen, "Numerical Investigation of the Effect of Baffle Orientation on Heat Transfer and Pressure Drop in a Shell and Tube Heat Exchanger With Leakage Flows," *Heat Transf. Eng.*, vol. 30, no. 14, pp. 1123–1135, 2009.

[22] R. K. Sinnott, *Chemical Engineering Design*, 4th ed. Butterworth-Heinemann, Oxford: Coulson & Richardson's Chemical Engineering, Elsevier, 2005.

[23] Y. You, Y. Chen, M. Xie, X. Luo, L. Jiao, and S. Huang, "Numerical simulation and performance improvement for a small size shell-and-tube heat exchanger with trefoil-hole baffles," *Appl. Therm. Eng.*, vol. 89, pp. 220–228, 2015.

[24] D. C. Wilcox, *Turbulence modeling for CFD*, 3rd ed. California: DCW Industries, 2006.

[25] J. C. Tannehill, D. A. Anderson, and R. H. Pletcher, *Computational fluid mechanics and heat transfer*, 2nd ed. Washington: Taylor and Francis, 1997.

[26] COMSOL, *CFD module user's guide*. COMSOL AB, 2013.

[27] O. C. Zienkiewicz and R. L. Taylor, *The Finite Element Method: Fluid Dynamics*, vol. 3. Oxford: Butterworth and Heinemann, 2000.

[28] M. O. Petinrin, A. A. Dare, and G. O. Asaolu, "Finite Element stabilization methods and solvers for heat exchanger applications: a review," in *Proceedings of International Conference of Mechanical Engineering, Energy Technology and Management*, 2016, pp. 977–987.